Article:
da Costa, E.B., Rodríguez, E.D., Bernal, S. et al. (2016) Production and hydration of calcium sulfoaluminate-belite cements derived from aluminium anodising sludge. Construction and Building Materials, 122. pp. 373-383. ISSN: 0950-0618

https://doi.org/10.1016/j.conbuildmat.2016.06.022

Preprint of a paper published in *Construction and Building Materials*, 122(2016):373-383.
Version of record is available at http://dx.doi.org/10.1016/j.conbuildmat.2016.06.022

Production and hydration of calcium sulfoaluminate-belite cements derived from aluminium anodising sludge

Eugênio Bastos da Costa[1], Erich D. Rodríguez[1,2*], Susan A. Bernal [3,4]; John L. Provis[3], Luciano Andrade Gobbo[5], Ana Paula Kirchheim[1]

[1] NORIE/UFRGS - Building Innovation Research Unit, Department of Civil Engineering, Universidade Federal Rio Grande do Sul, Porto Alegre, Brazil.

[2] Polytechnic School of Civil Engineering, IMED, Passo Fundo, Brazil.

[3]Department of Materials Science and Engineering, The University of Sheffield, Sheffield S1 3JD, United Kingdom

[4] Department of Civil and Structural Engineering, The University of Sheffield, Sheffield S1 3JD, United Kingdom

[5] PANalytical, São Paulo, Brazil.

*Corresponding author: erich.rodriguez@ufrgs.br

Abstract

Calcium sulfoaluminate-belite cement (CSAB) offers lower CO_2 emissions in its production, compared with Portland cement. However, for the production of CSAB a high amount of alumina is required, and the scarcity and high cost of high-purity bauxite make these cements costly at present. In this study, the use of uncalcined aluminium anodising sludge (AAS) as the main source of alumina to produce CSAB clinkers, replacing bauxite, was assessed. The CSAB clinkers produced were mainly composed of ye'elimite and belite, along with minor traces of alite, and/or brownmillerite, depending on the alumina source. Clinkers derived from AAS as a source of aluminium showed a lower content of ye'elimite (35.5%), as well as the

formation of alite (8.2%) when compared to a reference clinker produced with reagent-grade materials. Comparable hydration products were identified in the hydrated cements independent of the alumina source used. The use of AAS to produce CSAB cement was proven to be technically feasible, and the cement thus produced has desirable technical characteristics, presenting high mechanical strength (>40 MPa in paste samples).

Keywords: Calcium sulfoaluminate cement; clinker; hydration; anodising sludge; waste valorisation.

1. Introduction

Calcium sulfoaluminate (CSA) cements are based on the hydraulic phase tetracalcium trialuminate sulfate ($C_4A_3\bar{S}$ in cement chemistry notation), also known by the mineral name ye'elimite, as a major constituent [1–4]. As minor constituents, belite (C_2S), tricalcium aluminate (C_3A), calcium sulfosilicates (sulfospurrite or ternesite, $C_5S_2\bar{S}$), Al-rich ferrite (C_4AF) and calcium silico-aluminates (e.g. gehlenite, C_2AS) can also be present in these clinkers [5–7]. When the composition of the raw materials, the raw mix design or the clinkering processes change, some clinkers with different chemical and mineral compositions can also be generated, e.g. calcium-sulfoaluminate-belite (CSAB) cements containing mainly $C_4A_3\bar{S}$ and belite [3,8]; belite-rich cements containing both calcium sulfoaluminate and ferrite phases [8–12]; belite calcium-sulfoaluminate-ternesite cement [13,14], among others. The main difference between these cements and Portland cement (PC) is the low concentration or absence of tricalcium silicate (C_3S, alite) in CSA based clinker, and its higher content of sulfates.

Glasser and Zhang [15] proposed a hydration model for calcium sulfoaluminate binders. The high reactivity of $C_4A_3\bar{S}$ with calcium sulfates and water leads to rapid setting and

formation of ettringite ($C_6A\bar{S}_3H_{32}$), calcium monosulfoaluminate hydrate ($C_4A\bar{S}H_x$ where x is approximately 10-19; often termed SO_4-AFm or 'monosulfate'), and amorphous aluminium hydroxide (AH_3) (Eq. 1 and 2, respectively) as the main hydration products, which contribute to high early strength [16].

$$C_4A_3\bar{S} + 18H \rightarrow C_4A\bar{S}H_{12} + 2AH_3 \quad \text{(Eq. 1)}$$

$$C_4A_3\bar{S}+2C\bar{S}H_2+34H \rightarrow C_6A\bar{S}_3H_{32}+2AH_3 \quad \text{(Eq. 2)}$$

The relative quantities of ettringite and SO_4-AFm formed are related to the ratio of sulfate to aluminate present during the reaction. Other hydrate products identified include additional AFm-type phases (calcium carboaluminate hydrates or strätlingite), and hydrogarnet-type phases (mainly siliceous hydrogarnet) [1,16–20]. The understanding of the hydration mechanism and products of CSA cements have been advanced by Winnefeld and Lothenbach [17] through thermodynamic modelling, predicting the formation of ettringite and amorphous $Al(OH)_3$ from the hydration of ye'elimite. As the content of calcium sulfate decreases, monosulfate forms, along with the depletion of Ca and sulfate. If belite is present (as in CSAB cements), strätlingite is also formed as a secondary hydrate product [17].

The main applications for CSA-based cement, or its blends with Portland cement (PC), are in the production of self-stressed concrete elements, high early strength concretes for pre-cast products, cold weather concrete products, glass-fibre-reinforced composites and self-levelling floors [21,22]. CSA-based cement has been also used for the immobilisation of hazardous materials due to its low permeability and dense structure when hydrated [23].

CSA-based clinkers are generally produced by calcination of limestone, bauxite and gypsum, under conditions tailored to yield a desirable composition of the final

clinker [8,24]. These cements may be considered as a more sustainable alternative to PC due to the lower energy consumption and reduced CO_2 emissions associated with their production, as a result of the reduced limestone content required compared to PC [24]. CSA-based cements only release 0.216 g of CO_2/mL of the cementing phase, which is considerably lower than alite-based cements, the production of which emits 0.578 g of CO_2/mL [3]. The temperature of calcination is also around 200 ºC lower than is commonly used for PC production [14,25]. The low energy required for its grinding process, due to the friable clinker [4,14], also reduces the energy necessary for producing CSA-based cements [26,27].

CSA-based cement has been manufactured and successfully used since the 1970s in China, and also produced on a more limited scale in the E.U. and the U.S. [1,28]. Although in the past its worldwide production was relatively small, more recently major international companies have developed new products. For example, some industrial organisations are presenting new CSA cements based on recycled materials [29], and a new generation of low-carbon belite-rich sulfoferroaluminate cements has been patented under the name AETHER® [30], with a reduction of 25-30% in the emissions of CO_2 per tonne of cement when compared to PC. Various belite calcium sulfoaluminate ternesite (BCT) cements have also been patented since 2011 [31].

With a global production of 234 M metric tonnes annually [32], bauxite is a valuable resource for many industries, mainly for the production of alumina for manufacturing of aluminium metal. Global bauxite resources are estimated to be 55 to 75 billion tonnes, which are distributed in Africa (32%, Oceania (23%), South America and the Caribbean (21) and Asia (18%) [33]. Even though there exist relatively abundant available sources, the high demand for bauxite, as well as the costs related to its transport, reduce its

economic viability as a raw material for the manufacture of cements. This elucidates the challenges facing its potential use as a raw material in the production of CSA clinkers. Therefore, there is an imminent need to seek alternative alumina sources, such as Al-rich wastes or industrial by-products, to enable the cost-competitive production of these cements. Different industrial wastes or by-products with high contents of CaO, SO_3, and Al_2O_3, including fly ashes, blast furnace slag, phosphogypsum wastes, galvanising sludge, baghouse ash, and red mud have been used for the laboratory production of CSAB clinkers [9,24,34–38].

Aluminium anodising sludge (AAS) is an industrial waste produced during the electrochemical process of anodising aluminium. The solid waste obtained from this process is a sludge with a high content of aluminium hydroxide ($Al(OH)_3$), and other compounds including aluminium sulfate, sodium or calcium hydroxide can also be present. According to the Brazilian standard ABNT NBR 10004:2004 [39], this waste can be considered as a non-hazardous material, and it has been used as a source of Al_2O_3 in the production of mullite-based ceramics [40,41]. The high amounts of this waste produced (100 kt/year in the EU and ~1500 kt/y in Brazil), and the lack of a full pathway for its re-use, raise environmental concerns [42]. The assessment of AAS as a raw material for the production of a belitic cement (without the presence of ye'elimite-type phases) was previously reported by Pereira *et al* [43,44], but the use of AAS as a source of Al_2O_3 in the synthesis of CSAB-type cement (whose clinker contains belitic and ye'elimite phases) has not been studied. Therefore, it is not fully understood whether the differences between chemical compositions and presence of minor elements between bauxite and AAS will have a significant effect during the synthesis of CSAB-type cements, and the hydrated products formed from the clinkers derived from this waste have not been assessed in detail.

The aim of this study is to assess the potential use of an aluminium anodising sludge as an alternative source of Al_2O_3, instead of bauxite, in the production of CSAB clinkers. The effect of partial and total substitution of bauxite by AAS on the final phase assemblage obtained during the synthesis of CSAB clinkers were assessed, to identify if the use of alternative sources of Al_2O_3 during the synthesis modifies the clinker phase assemblages formed. The hydration products formed from these clinkers were also assessed using X-ray diffraction (XRD), thermogravimetric analysis (TGA) and ^{29}Si and ^{27}Al solid state magic angle spinning nuclear magnetic resonance spectroscopy (MAS-NMR). The hydration kinetics were studied through isothermal conduction calorimetry (ICC), and the compressive strength development during curing was also determined.

2. Experimental Procedure

2.1. Materials

For the production of the CSAB clinkers two different sources of alumina were used: an aluminium-anodising sludge with 70.0% H_2O supplied by Alcoa (Tubarão, Brazil), and a bauxite-rich mineral from Curimbaba (São João Del Rei, Brazil). Limestone was supplied by Cimpor Cement (Candiota, Brazil). The other raw materials, used mainly for sintering the reference clinker, were analytical grade: $CaCO_3$, Fe_2O_3, Al_2O_3, $CaSO_4 \cdot 2H_2O$, and $SiO_2 \cdot xH_2O$ supplied from Dinâmica Contemporânea Ltda. The chemical compositions of the raw materials are shown in Table 1.

Preprint of a paper published in *Construction and Building Materials*, 122(2016):373-383.
Version of record is available at http://dx.doi.org/10.1016/j.conbuildmat.2016.06.022

147 Table 1 Chemical compositions of raw materials used (wt.%, from X-ray fluorescence)

Raw Material	SiO_2	Al_2O_3	Fe_2O_3	SO_3	CaO	MgO	Na_2O	K_2O	Cl^-	TiO_2	P_2O_5	LOI*	Other
Calcium sulfate†	--	--	--	46.4	32.5	-	--	--	--	--	--	21.1	-
Silicon oxide†	83.6	-	-	-	-	-	-	-	-	-	-	16.4	-
Ferric oxide†	--	--	96.5	--	--	--	--	--	--	--	--	3.5	--
Aluminium oxide†	-	96.5	-	-	-	-	-	-	-	-	-	3.5	-
Calcium carbonate†	-	-	-	-	56.0	-	-	-	-	-	-	44.0	-
Limestone	12.9	2.3	1.4	0.1	41.2	4.0	-	0.7	-	0.1	0.2	37.0	0.3
Bauxite (Bx)	10.0	75.0	12.7	-	-	0.1	-	0.2	-	1.1	0.1	0.2	0.6
Aluminium anodising sludge (AAS)**	1.9	73.6	0.5	20.5	0.6	0.2	1.2	0.2	0.1	-	0.5	-	0.7

148 †Analytical grade *Loss on ignition at 1050 ºC. **Dried at 100 ºC for 24 h

149

150 *2.2. Synthesis of CSAB clinker*

151 The CSAB clinkers were formulated according to the Bogue-type equations procedure
152 suggested by Majling *et al.* [45], with the raw meal mixes designed to obtain similar
153 oxide compositions and a phase assemblage based on 40% C_2S, 40% $C_4A_3\bar{S}$, 10% C_4AF
154 and 10% $C\bar{S}$, while other minor clinker phases are predicted to be negligible [24,25].
155 The proportions of the raw materials, and clinker IDs, are shown in Table 2. The
156 reference clinker (CSAB-Ref) was formulated and produced with reagent grade
157 materials. Total and partial substitution of bauxite by AAS was carried out in order to
158 assess the effect of Al_2O_3 source on the final properties of the clinker produced.

159 Table 2 Formulations used for the synthesis of CSAB clinkers (wt.%)

Raw Materials	Clinker ID		
	CSAB-Ref	CSAB-Bx/AAS	CSAB-AAS
Calcium carbonate (reagent grade)	51.1	1.1	-
Calcium sulfate (reagent grade)	17.5	11.9	7.3
Aluminium oxide (reagent grade)	16.8	-	-
Silicon oxide (reagent grade)	12.2	-	0.2
Ferric oxide (reagent grade)	2.5	-	1.1

Limestone	-	68.6	72.9
Bauxite (Bx)	-	9.2	-
Aluminium anodising sludge (AAS)*	-	9.2	18.5

*Dried at 100 ºC for 24 h

The raw materials (100% passing 75 µm) were dried at 100 ºC for 24 h, homogenised using a ball mill for 1 h (balls:powder mass ratio 1:5, 60 rpm) and then pelletised (moulded manually into spherical pellets with a moisture content of 30% and diameter ~1 cm). After drying in an oven (100 °C for 24 hours) the pellets were heated at 900 ºC for 30 min and then sintered at 1250 ºC for 30 min in a static laboratory muffle furnace with a heating rate of 5 ºC/min, followed by quenching with forced air convection. The clinkers were then ball milled and sieved to 100% passing 45 µm.

The particle size distributions of the ground clinkers were analysed using a laser granulometer 1180 (CILAS). Mineralogy was analysed by X-ray diffraction using a PANalytical Empyrean diffractometer with Cu Kα (λ=1.5418 Å) radiation, a step size of 0.013º, 97.92 s count time per step (~30 min data collection per scan). Quantitative analysis was performed through Rietveld analysis using the X´Pert High Score Plus software (PANalytical), with goodness-of-fit calculated to be better than 3.3 and Weighted R profile maximum 7.3%. Structural data for alite [46], belite [47], ferrite [48], cubic ye'elimite [49], orthorhombic ye'elimite [50], ternesite [51], anydrite [52], and periclase [53] were used for refinement and quantification of the anhydrous crystalline phases. X-ray fluorescence data were collected using an Axios Advanced spectrometer (PANalytical) via standardless semiquantitative analysis. Loss on ignition was performed at 1050 ºC for 1 h in air.

2.3. Tests conducted on pastes

Pastes using the three CSAB clinkers synthesised (CSAB-Ref; CSAB-Bx/AAS; and CSAB-AAS) were produced with a water/binder ratio of 0.45, following Chen and Juenger [25] and Jewell *et al.* [54]. The hydration process of the CSAB clinkers was assessed by isothermal conduction calorimetry using a TAM Air calorimeter (TA Instruments). The mixtures were hand mixed for 5 min and then placed into the calorimeter. The heat evolution was evaluated for 24 h at 23 ºC.

The compressive strength development was assessed in 13 mm cubic paste samples, cured under saturated limewater at 25 ºC due to the high content of belite in the clinker. The compressive strength was determined after 3, 7, and 28 of curing according to the method proposed by Mehta and Gjorv [55], using a universal testing machine UH-F2000KN (Shimadzu) with a loading rate of 0.2 MPa/s. The results reported correspond to the mean of four replicate samples tested for each formulation.

The hydrated samples were crushed, treated with isopropanol to prevent further hydration, filtered, and stored in a sealed container until testing. The hydration products were evaluated through:

- X-ray diffraction (XRD), as described for the anhydrous clinker phases above.
- Thermogravimetric analysis using a Mettler Toledo TGA/TSO SDTA 851e, under a flow rate of 40 mL/min of nitrogen and a heating rate of 10 °C/min up to 1000 °C.
- Solid-state ^{29}Si MAS NMR; spectra were collected at 59.56 MHz on a Varian Unity Inova 300 (7.05 T) spectrometer using a probe for 7.5 mm o.d. zirconia rotors and a spinning speed of 5 kHz. The ^{29}Si MAS experiments employed a 90° pulse of duration 5 µs, a relaxation delay of 5 s and 14000 scans. Solid-state ^{27}Al MAS NMR spectra were acquired at 104.198 MHz, using a Varian VNMRS 400 (9.4 T) spectrometer and a probe for 4 mm o.d. zirconia rotors and a spinning speed of 14 kHz with a pulse

206 width of 1 μs (approximately 25°), a relaxation delay of 0.2 s, and a minimum of 7000
207 scans. ^{29}Si and ^{27}Al chemical shifts are referenced to external samples of
208 tetramethylsilane (TMS), and a 1.0 M aqueous solution of $Al(NO_3)_3$ respectively.

209 3. Results and Discussion

210 *3.1. Characterisation of CSAB clinkers*

211 The chemical compositions, obtained by XRF, of the clinkers produced are shown in
212 Table 3. The contents of CaO, Al_2O_3, SO_3, and Fe_2O_3 in the C$\bar{S}$AB clinkers after
213 sintering were similar for all samples, and the XRD phase quantification shows that the
214 clinkers were close to the target phase compositions (Table 4 and discussion below).
215 These results elucidate the effectiveness of the use of the Bogue method as modified by
216 Majling *et al.* [56] in designing CSAB clinkers using different raw materials. The slight
217 deviations can be attributed to the impurities contained in the mineral and waste
218 materials. The higher content of MgO of the clinkers produced with the alternative
219 alumina sources (CSAB-Bx/AAS and CSAB-AAS) can be attributed to the use of
220 limestone with an MgO content higher than 5 wt.% (Table 1). The content of Na_2O and
221 K_2O is also higher, especially for CSAB-AAS, due to the alkalis supplied by the AAS.

222 Table 3. Chemical compositions of CSAB clinkers produced (wt.%).

Compound	CSAB-Ref	CSAB-Bx/AAS	CSAB-AAS
CaO	48.9	49.8	51.2
Al_2O_3	16.9	16.0	15.1
SiO_2	16.8	11.1	9.7
SO_3	12.4	10.9	12.1
Fe_2O_3	3.7	3.7	3.3
MgO	0.1	5.6	5.1
Na_2O	0.4	0.4	0.8
K_2O	0	0.7	0.7
Cl	0.03	0.02	0.02
TiO_2	0	0.40	0.1
P_2O_5	0.02	0.1	0.1
Other components	0.18	0.40	0.29
LOI*	0.57	0.78	1.48

*Loss on ignition at 1050 ºC for 1 h.

The X-ray diffraction patterns of the anhydrous CSAB clinkers (Figure 1) and their corresponding results of Rietveld quantitative phase analysis (Table 4) show the presence of ye'elimite (both cubic and orthorhombic polymorphs, $Ca_3Al_6O_{12}{\cdot}CaSO_4$, Powder Diffraction File (PDF) cards # 01-071-0969 and # 01-085-2210, respectively) and belite (Ca_2SiO_4; PDF# 01-086-0398). The absence of free lime indicates a complete conversion to the CSAB clinker phases, when either reagent-grade raw materials, natural (Bx), or waste materials (AAS) were used. Ternesite ($Ca_5(SiO_4)_2(SO_4)$; PDF# 01-088-0812), anhydrite ($CaSO_4$; PDF#00-003-0162), a substituted aluminoferrite-type phase (brownmillerite-type structure, approximated for brevity as C_4AF), PDF# 01-087-1229) and alite ($3CaO{\cdot}SiO_2$, PDF# 01-086-0402), were identified. Periclase (MgO, PDF# 00-003-0998) was observed only in the CSAB-Bx/AAS and CSAB-AAS clinkers. The formation of alite can be attributed in part to the presence of MgO in the limestone [57], which was only used for the synthesis of the CSAB-Bx/AAS and CSAB-AAS clinkers. Liu *et al.* [57] reported that the presence of a suitable amount of

238 MgO (>0.5%) can promote the formation of C_3S at lower temperatures and is beneficial
239 for its coexistence with $C_4A_3\bar{S}$. The higher content of P_2O_5 in the raw meal mixes used
240 for the production of CSAB-Bx/AAS and CSAB-AAS might have an effect on the
241 synthesis of C_2S, C_3S and $C_4A_3\bar{S}$. The stabilization of β-C_2S has been identified,
242 indicating that the clinkering and cooling processes were properly performed [58,59].
243 Traces of calcite ($CaCO_3$; PDF# 00-002-0623) are also identified, as a consequence of
244 possible carbonation of the samples during storage and analysis.

245 The percentages of the main clinker phases ($C_4A_3\bar{S}$, C_2S and C_4AF) are very similar to
246 the expected values from the Bogue-type calculations. The CSAB-Ref exhibited a
247 higher amount of ye'elimite (the sum of the orthorhombic and cubic structures) than the
248 other CSAB clinkers. However, as the content of AAS used in the production of CSAB
249 increases, the ratio of orthorhombic to cubic ye'elimite is also higher. CSAB-Ref
250 showed the lowest cubic-$C_4A_3\bar{S}$ /orthorhombic-$C_4A_3\bar{S}$ ratio (0.094) when compared to the
251 CSAB clinkers derived from AAS (0.20 and 0.23 for CSAB-Bx/AAS and CSAB-AAS,
252 respectively). Bullerjahn *et al.* [14] reported a higher content of cubic ye'elimite at the
253 expense of the orthorhombic form with increasing Fe content. Although the differences
254 in iron content between the clinkers CSAB-Ref and CSAB-Bx/AAS appear negligible,
255 the crystallisation of the cubic polymorph might be promoted by the presence of foreign
256 ions, including Na^+, K^+, Mg^{2+}, and Ti^{4+}, which are present in higher concentrations in
257 CSAB-Bx/AAS clinker, Table 3. Hargis *et al.* (2014) [60] identified, using Rietveld
258 refinements for cubic, orthorhombic, and tetragonal crystals, that the peak intensities
259 and positions of the orthorhombic crystal structure best match pure $C_4A_3\bar{S}$

260

261 Table 4. Rietveld quantitative phase composition of the CSAB clinkers produced.

262 Values reported in mass percentages

	CSAB-Ref	CSAB-Bx/AAS	CSAB-AAS
Orthorhombic ye'elimite ($C_4A_3\bar{S}$)	37.0	25.5	28.8
Cubic ye'elimite ($C_4A_3\bar{S}$)	3.5	5.3	6.7
Total ye'elimite (cubic + orthorhombic)	40.5	30.8	35.5
Belite (C_2S)	32.1	41.1	39.1
Ternesite ($C_5S_2\bar{S}$)	19.3	--	--
Brownmillerite-type phases (C_4AF)	4.6	11.9	7.4
Anhydrite ($C\bar{S}$)	3.5	2.0	4.0
Alite (C_3S)	--	7.7	8.2
Periclase (MgO)	--	6.5	5.9
Agreement indices			
R expected - R_{exp} *(%)*	4.1	4.1	4.1
Weighted R profile - R_{wp} *(%)*	7.3	6.0	6.4
Goodness of fit – $\chi^2 = \left[\frac{R_{wp}}{R_{exp}}\right]^2$	3.2	2.2	2.4

263 *Loss on ignition at 1050 ºC.
264

Preprint of a paper published in *Construction and Building Materials*, 122(2016):373-383. Version of record is available at http://dx.doi.org/10.1016/j.conbuildmat.2016.06.022

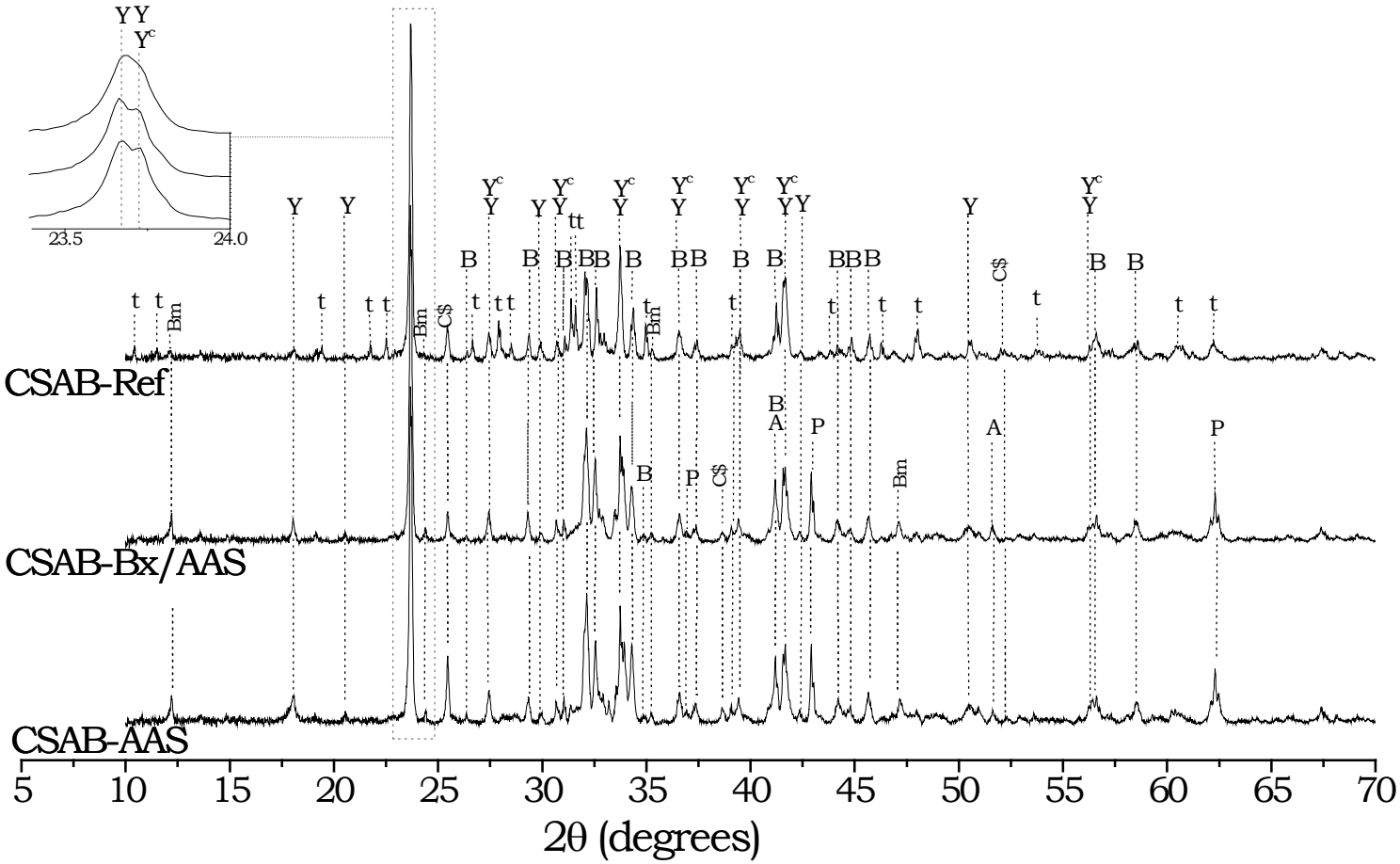

Y: orthorhombic ye'elimite; Y^c: cubic ye'elimite; B: belite; t: ternesite; Bm: brownmillerite; C$: anhydrite; A: alite; P: periclase

Figure 1. X-ray diffractograms of anhydrous CSAB clinkers

A calcium sulfosilicate with a ternesite-type structure ($Ca_5(SiO_4)_2(SO_4)$; $C_5S_2\bar{S}$) was identified only in CSAB-Ref, which also has the lowest C_4AF and β-C_2S contents. Ternesite is an intermediate phase generally present at temperatures between 1100 and 1180 °C during the crystallisation of belite in CSAB cements, whose formation is strongly affected by the content of SO_3, the presence of mineralisers (including phosphates or fluorides) and/or the cooling rate from 1250 to 800 °C [14,61]. Taking into account that quenching from ~1200 °C was applied after clinkerisation, and that the contents of SO_3 among the clinkers assessed here are similar, the sulfate supplied by the AAS (which is ~20%, Table 1) might have higher availability during the synthesis than the sulfate provided as anhydrite. The minor oxides (MgO, TiO_2, K_2O) supplied by the limestone, bauxite and AAS promoted the formation of alite in CSAB-Bx/AAS and CSAB-AAS. Ternesite formation occurred under conditions of the absence of such mineralizing elements and higher availability of SiO_2.

The particle size distributions of the CSAB clinkers obtained after mechanical treatment do not exhibit significant differences, Figure 2.

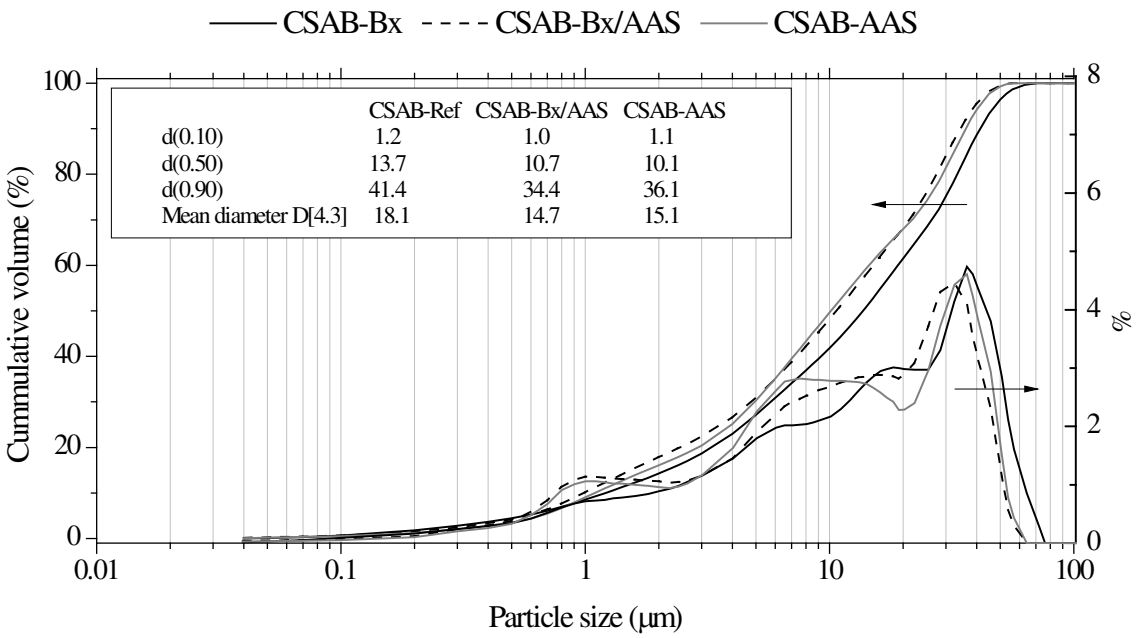

Figure 2. Particle size distributions of CSAB clinkers.

3.2. Phase evolution during hydration of CSAB clinkers

3.2.1. Isothermal calorimetry

The heat release profiles during the hydration of the clinkers show two distinct peaks (Figure 3); the first appears during the initial five minutes of reaction and the second is after 0.5-2 hours. CSAB-Ref showed a third peak after 8 h (Figure 3A), which is tentatively attributed to the formation of additional ettringite as hydration continues, but this was not observed for the other clinkers (Figure 3B,C).

The CSAB-Bx/AAS and CSAB-AAS clinkers show the highest heat release rate during initial hydration (~27 mW/g binder), 2 minutes after loading into the calorimeter (7 minutes after the start of mixing), followed by CSAB-Ref, although the data obtained during this very early period must be treated as semi-quantitative due to the requirement for stabilisation of the calorimeter after loading. The second peak located after ~1 h for CSAB-AAS is more intense (maximum heat evolution rate 31 mW/g binder) compared with the corresponding peak for CSAB-Bx/AAS, which is present at 40 min and with

lower intensity (maximum rate 12 mW/g binder). Considering that the clinkers showed similar particle size distributions (Figure 2), the effect of fineness on the differences identified in the hydration rates should be negligible. Thus, the heat evolution is likely to be dependent on clinker composition. The heat released during the first minutes is higher than for traditional OPC systems due to the higher content of rapidly soluble sulfates, and the fast dissolution of ye'elimite and other reactive phases when the particles come into contact with water [17]. Hargis *et al.* [60] reported that ye'elimite exhibits a relative low bulk modulus (~69 GPa), which can be attributed to its open aluminate framework as well as the high charges on the cation Ca^{2+} and anion SO_4^{2-} in intraframework sites. This increases its internal energy, and therefore its reactivity with water.

The absence of gypsum from the CSAB cements contributes to its high reactivity and accelerates the point of maximum heat release. The second peak, also described as the main hydration peak, corresponds to the reaction of ye'elimite ($C_4A_3\bar{S}$), and also some C_4AF, with calcium sulfate to form ettringite ($C_6A\bar{S}_3H_{32}$) and amorphous aluminium hydroxide (AH_3) (Eq. 1 and 2) [17].

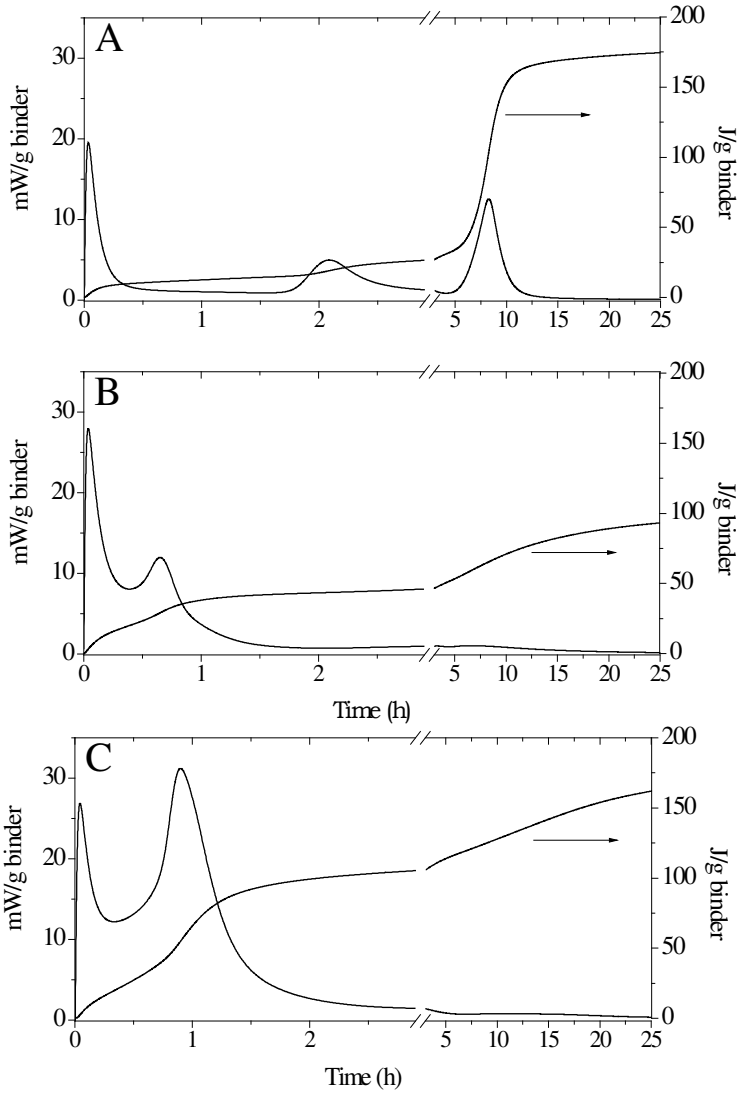

316

317 Figure 3. Isothermal calorimetry curves for clinker pastes. A. CSAB-Ref, B. CSAB-
318 RBX/AAS, and C. CSAB-AAS. In each plot, the left-hand vertical axis shows the rate
319 of heat release, and the right-hand vertical axis shows the cumulative heat release.

320

321 The different crystal structures identified for the ye'elimite polymorphs in each of the
322 clinkers synthesised may also contribute to the differences in their kinetic behaviour.
323 Cuesta *et al*. (2014) [20] assessed the reactivity of the polymorphs of synthetic
324 ye'elimite, where the orthorhombic ye'elimite reacts more slowly than the cubic
325 ye'elimite. Such behaviour is aligned with the results reported here, as the CSAB-AAS

showed the highest heat release in the first 4 h due to its higher cubic ye'elimite content (Table 4); a higher cubic/orthorhombic ye'elimite ratio is observed when AAS is used in the raw meal mixes. On this basis, the lower reactivity of CSAB-Ref (mainly at early age) cannot be attributed solely to the presence of ternesite in this clinker. Ternesite has been also identified as a secondary phase in CSAB clinkers [13,14,31,34,62,63], where contradictory results regarding its hydration behaviour are reported. Ternesite is often considered to decrease the setting rate of CSAB, potentially acting as an inert phase with very low reactivity degree [64–67]. However, the aluminium released during ye'elimite hydration has a strong influence on ternesite reactivity, as the dissolution rate of ternesite is affected by the presence of soluble sulfate sources ($C\bar{S}$ or $C\bar{S}H_2$) and the availability of $Al(OH)_4^-$ within the pore solution [14,31,68].

The evolution of heat during hydration of CSAB-Ref shows a second heat release up to 1.5 h, which is considerably delayed compared with the CSAB-Bx/AAS and CSAB-AAS clinkers, where this period only lasts around 25 min. Although the CSAB-Ref exhibited the lowest maximum heat release in the first two hours of reaction, its cumulative heat of hydration after 24 h was 172.3 J/g, which is higher by 48% and 11% than the corresponding data obtained for CSAB-Bx/AAs and CSAB-AAs, respectively (Figure 3B,C).

3.2.2. X-ray diffraction analysis of hydrated CSAB clinkers

Figure 4 shows the XRD pattern in a 2θ range between 6 and 25 degrees for the hydrated pastes up to 28 days of curing. As main crystalline hydration products in the CSAB pastes, ettringite ($Ca_6Al_2(SO_4)_3(OH)_{12}{\cdot}26H_2O$; $C_6A\bar{S}_3H_{32}$, PDF# 00-031-0251) and SO_4-AFm ($Ca_4Al_2SO_{10}{\cdot}12H_2O$; PDF# 00-045-0158) were identified. At 28 days, the consumption of ye'elimite, as well as the presence of belite and AH_3 (which would

be present as an amorphous phase) lead to the crystallization of a strätlingite-type AFm phase ($Ca_2Al_2SiO_7 \cdot 8H_2O$; PDF# 00-029-0285). Residual crystalline phases in non-hydrated $C\bar{S}AB$ clinker grains, such as ye'elimite, belite, and ternesite, were identified in the hydrated paste at all ages assessed. These results are in accordance with other reports where residual ye'elimite has been identified in hydrated pastes even after 360 days of curing [69].

The higher degree of consumption of ye'elimite during the hydration of CSAB-AAS than the other samples tested is evident from the XRD analysis (more evident in the data for 1 day samples, and related to the content of cubic ye'elimite which has high reactivity). These results are in good agreement with the fast dissolution of sulfate phases and subsequent ettringite precipitation identified through the higher heat release during the first minutes (Figure 3A). According to Chen and Juenger [24], and Jawed and Skalny [70], the dissolved alkali concentration during hydration could also increase for the CSAB-ASS and CSAB-Bx/ASS clinkers due to the release of Na^+ and K^+ from the reactive anhydrous phases, which increase the dissolution rate of aluminate phases (in particular $C_4A_3\bar{S}$) and the subsequent formation of ettringite and AH_3 phases.

Preprint of a paper published in *Construction and Building Materials*, 122(2016):373-383.
Version of record is available at http://dx.doi.org/10.1016/j.conbuildmat.2016.06.022

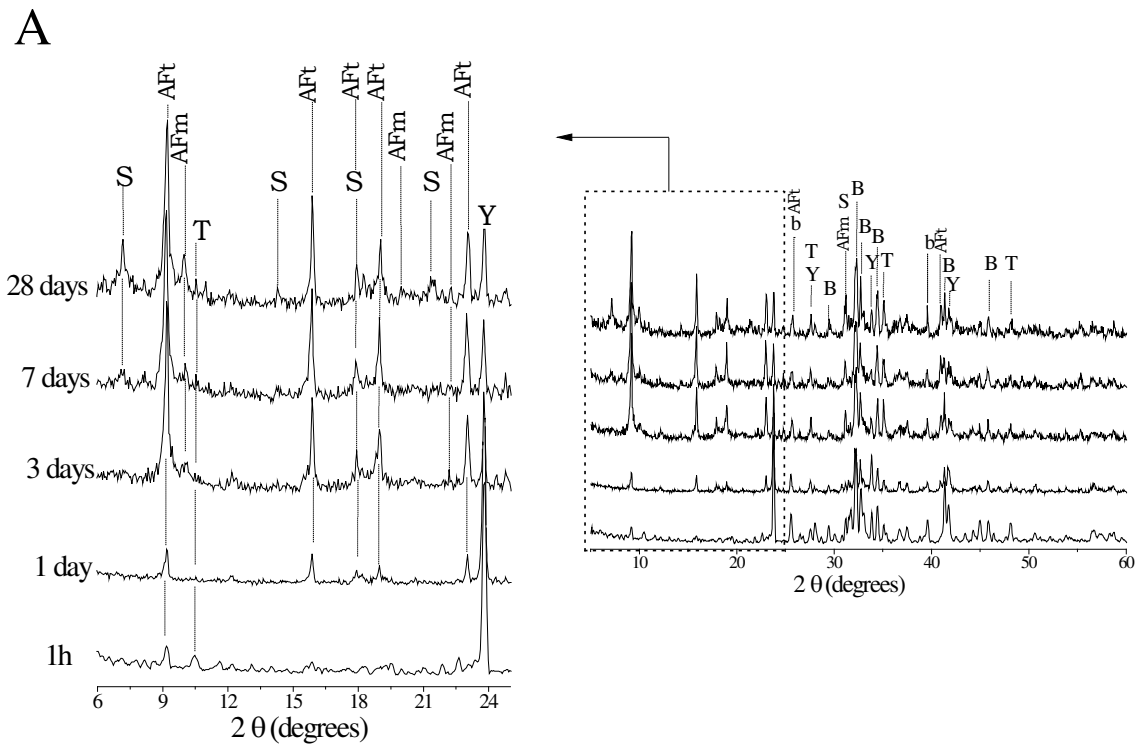

366

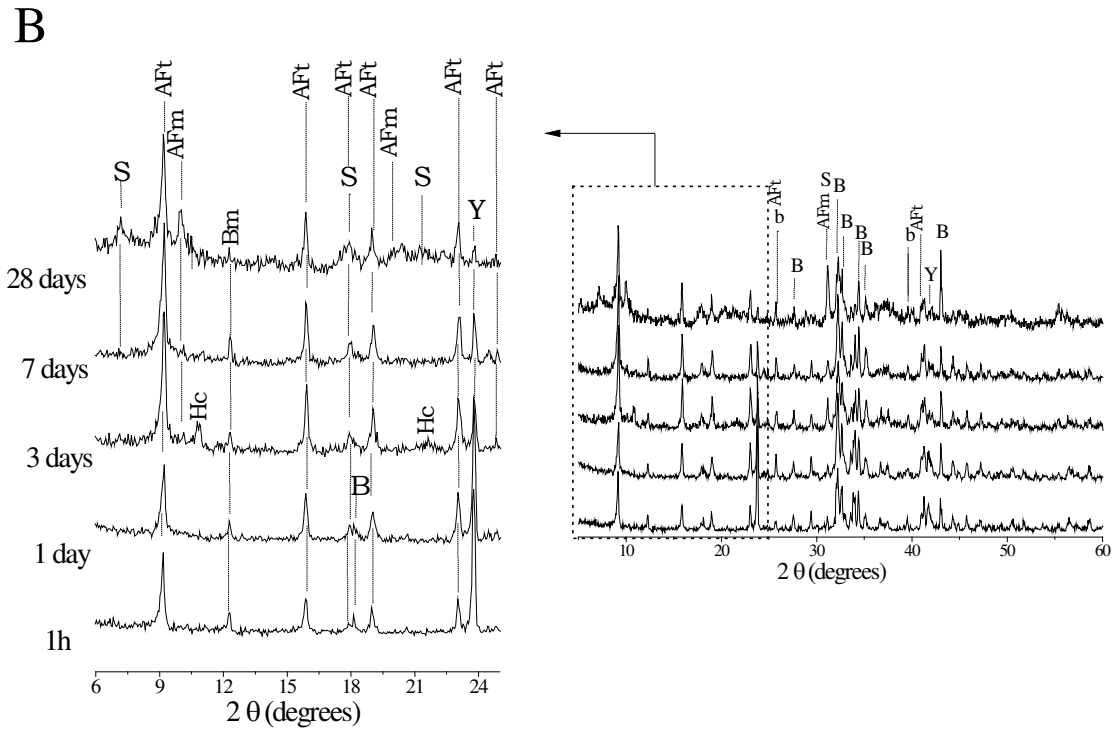

367

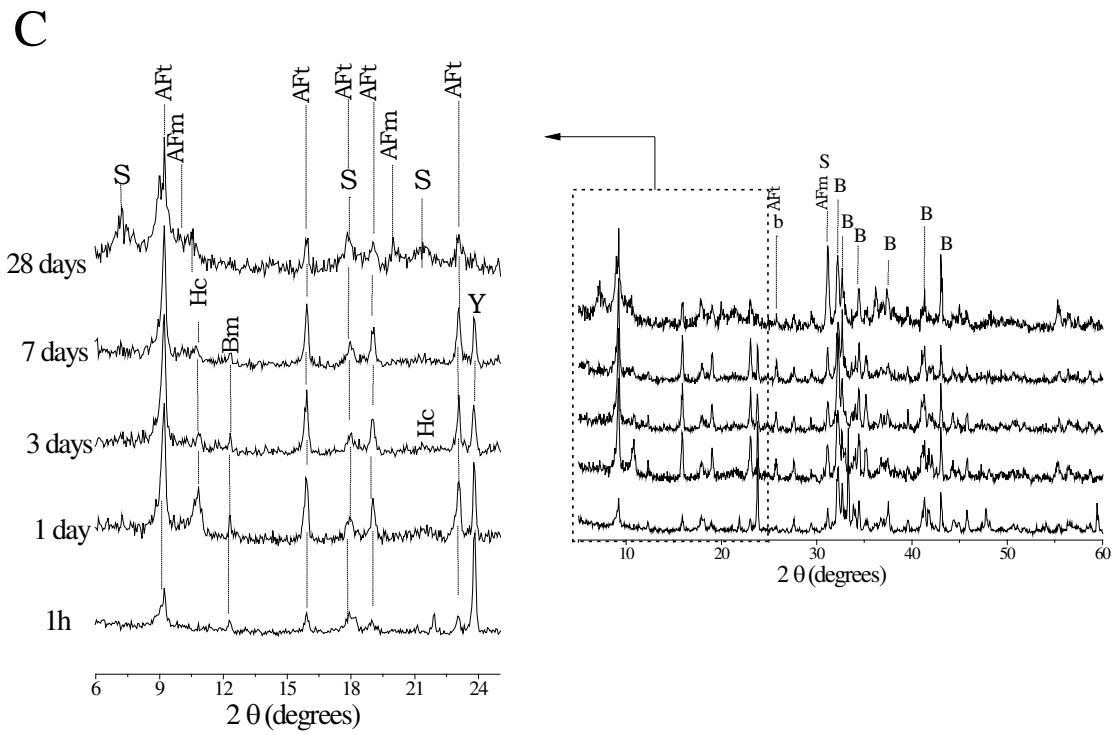

Y: ye'elimite; B: belite; T: ternesite; Bm: brownmillerite; AFt: ettringite; AFm: calcium monosulfoaluminate hydrate; Hc: calcium hemicarboaluminate hydrate; S: strätlingite.

Figure 4. X-ray diffractograms of hydrated pastes up to 28 days of curing. A. CSAB-Ref; B. CSAB-Bx/AAS; and C. CSAB-AAS.

After ettringite formation is close to complete – the corresponding XRD peaks exhibit the highest intensity after 3 days of curing – AFm products start to form. Contrary to other reports [14,16,18,19], portlandite (CH), hydrogarnet and calcium silicate hydrate were not identified as hydrate products here. The presence of belite, which acts as a silica source, as well as the $C_4A_3\bar{S}$ and/or AH_3 as aluminium sources, can lead to the formation of strätlingite [71], for example according to the equation $C_2S + AH_3 + 5H \rightarrow C_2ASH_8$ [17]. As the hydration proceeds, calcium hemicarboaluminate hydrate ($Ca_4Al_2(OH)_{12}(OH)(CO_3)_{0.5}\cdot nH_2O$; ($CO_3$,OH)-AFm, PDF # 00-036-0129) is formed from CSAB-Bx/AAS and CSAB-AAS clinkers after 3 days and 1 day of curing, respectively, but then was not identified at later ages. This suggests that the samples were taking up CO_2 from the ambient atmosphere, taking into account the slow kinetics

384 of dissolution of calcium carbonate [72], as well as the higher thermodynamic stability
385 of (CO_3,OH)-AFm phases compared to monosulfate [73].

386 The low reactivity of belite contributes to the low silica availability in these binders
387 during the early stages of reaction, and strätlingite is only detected after 7 days of
388 curing. At later age, further formation of strätlingite is identified. This phase can exhibit
389 low crystallinity, small crystal size and/or internal disorder during its crystallisation as
390 evidenced by the broad XRD peaks observed (Figure 4), particularly for CSAB-AAS
391 [74]. This higher degree of disorder can be attributed to the high affinity of strätlingite
392 for alkali metal cations, which reduce the regularity of its structure, and so this is
393 observed mainly for those clinkers with high contents of sodium and potassium [17].
394 Santacruz *et al* [75], reported that the microstructure of strätlingite can be also affected
395 by dehydration when the sample is dried for characterisation. This slight drying damage
396 changes the interlayer spacing, meaning that the main (003) peak can be broadened and
397 shifted.

398 According to Bullerjahn *et al.* [14], the presence of ternesite reduces C_2S reactivity
399 during the hydration of a belite calcium sulfoaluminate ferrite clinker. This is in good
400 agreement with the results presented here, where the CSAB-Ref, which contained 16%
401 ternesite, also showed lower formation of strätlingite than the other clinkers after 28
402 days of curing.

403 *3.2.3. Thermogravimetry*

404 The thermogravimetric analysis (Figure 5) shows a higher reactivity for C$\bar{S}$AB-Bx/AAS
405 than the other clinkers, as seen by the higher content of hydrated products formed.
406 C$\bar{S}$AB-Ref exhibited a total mass loss of ~20%, which is 19% less than that of CSAB-

Bx/AAS. The differential thermogravimetry (DTG) curves show a pronounced peak located at 110 °C corresponding to the loss of hydrate water from ettringite [76]. A second peak is identified at ~260 °C, associated with amorphous $Al(OH)_3$. The very similar position of this peak between CSAB-Bx/AAS and CSAB-Ref elucidates the similar environments of the bound water in these samples. According to Kuzel [77], the peak at 160 °C for the CSAB-Bx/AAS paste can be attributed to strätlingite, which exhibits three endothermic peaks, a minor peak at ~120 °C and main peaks at 165 and 220 °C. It is not possible to separately quantify the amount of ettringites and AFm-type phases, including strätlingite, from TGA as their temperatures of decomposition (30-180 °C) overlap [78]. The set of peaks located between 650 and 710 ºC are attributed to decomposition of carbonates formed due to superficial carbonation of the samples.

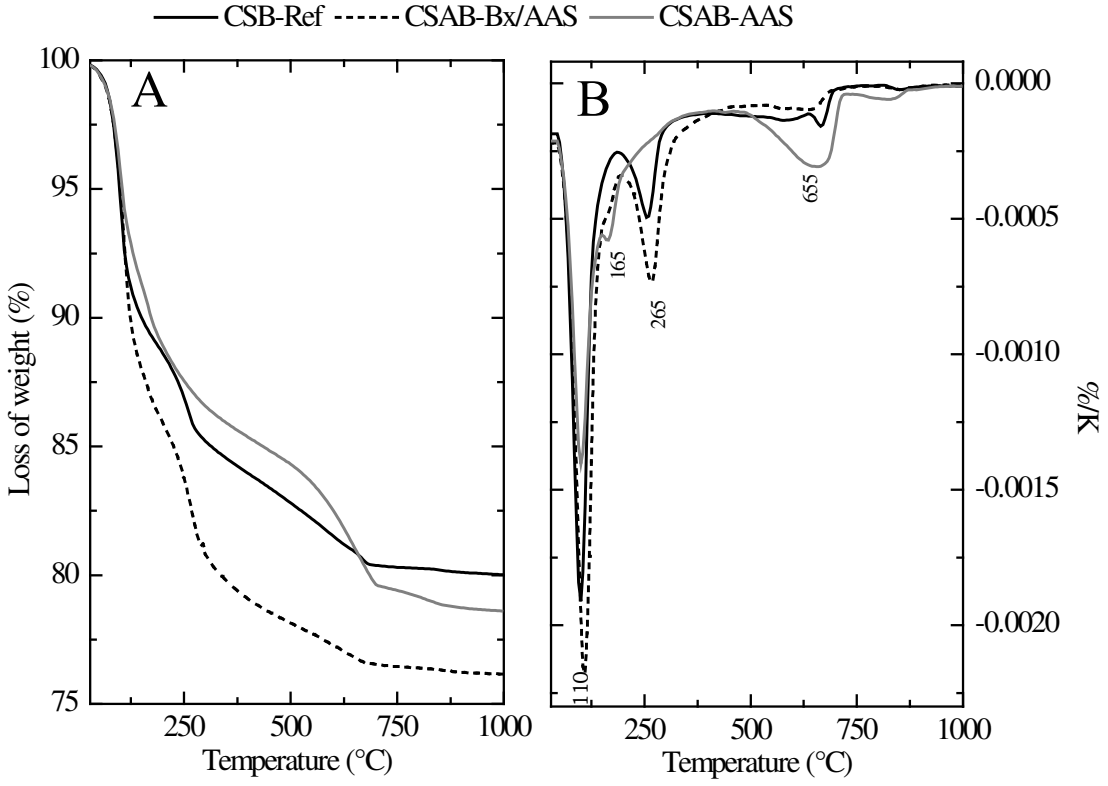

Figure 5. Thermogravimetric analysis for CSAB clinker hydration products after 28 days of curing.

422 *3.2.4. Solid-state NMR spectroscopy*

423 The ^{27}Al MAS NMR spectra for anhydrous clinkers and the pastes after 28 days of
424 curing are shown in Figure 6. The clinkers show a wide band with two signals located at
425 50 – 80 ppm, corresponding to structurally distinct tetrahedrally coordinated Al sites.
426 These signals can be attributed mainly to the ye'elimite, and any Al substituting for Si
427 in alite or belite will also contribute to the downfield region of this resonance [79]. The
428 Al present in the aluminoferrite phases identified by XRD does not contribute
429 considerably to the ^{27}Al MAS NMR spectra due to the high concentration of Fe^{3+}
430 present either in paramagnetic or antiferromagnetic form in this phase [80]. The effect
431 of Fe^{3+} on the ^{27}Al MAS NMR spectra of CSAB clinkers assessed here is not yet well
432 identified, especially due to the wide range of Al/Fe ratios present in the ferrite phases.
433 The signal of Al^{IV} for CSAB-Ref clinker is broad with a maximum located at ~68 ppm,
434 while the clinkers produced with alternative Al_2O_3 sources (CSAB-Bx/AAS and CSAB-
435 AAS) show a more intense peak, which also has a shoulder located at ~60 ppm. The
436 weak signal located at ~13 ppm for the clinkers can be attributed to the Al^{VI}, which is
437 either present as a guest ion in the belite phase [79], or the partial pre-hydration of the
438 ye'elimite through contact with atmospheric moisture.
439

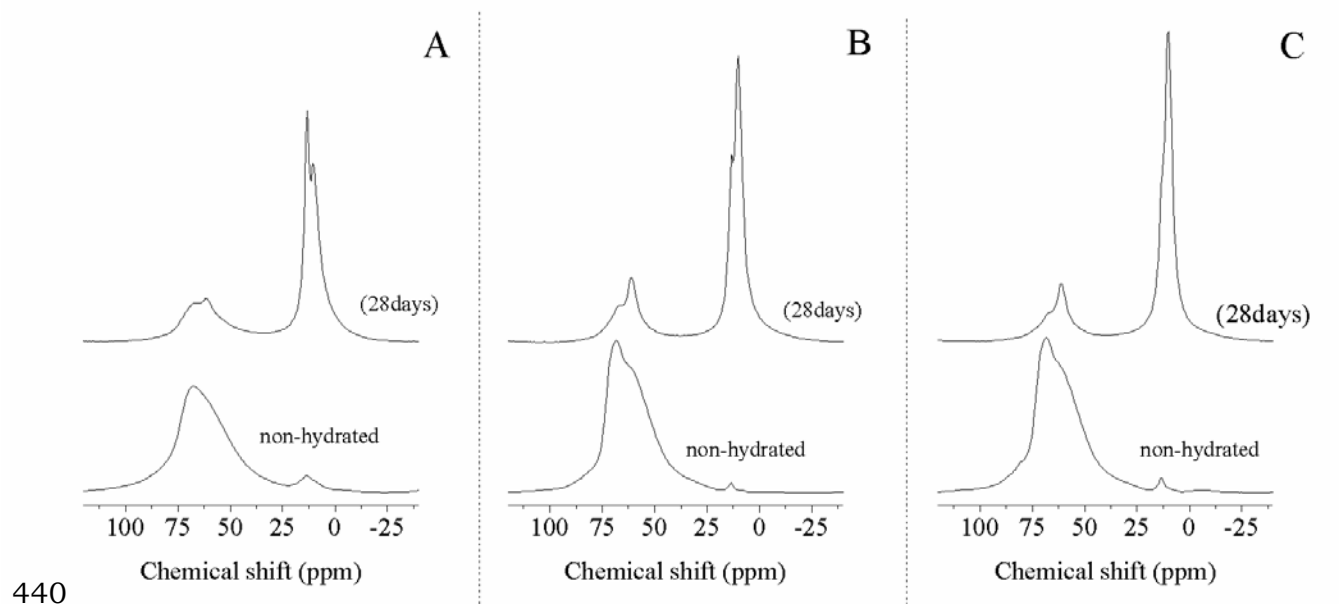

Figure 6. ^{27}Al MAS NMR spectra of anhydrous clinkers and CSAB pastes after 28 days of curing. A. CSAB-Ref; B. CSAB-Bx/AAS and C. CSAB-AAS.

The dissolution and subsequent hydration of reactive phases modify the molecular environment, and a more intense peak between 0 and 20 ppm is identified in the hydrated paste samples. The hydration reaction considerably reduces the signal attributed to Al^{IV}; instead, a narrower and very much intense Al^{VI} peak is obtained. This is associated with the ye'elimite dissolution and subsequent formation of ettringite whose octahedrally-coordinated Al is identified at ~13 ppm. The partially overlapping signal identified at ~10 ppm can be assigned to the AFm-type phases including strätlingite [81].

In the hydrated paste of CSAB-Bx/AAS, the peak attributed to the ettringite (~13 ppm) showed a lower intensity when compared to the AFm-type phases (~10 ppm), although these peaks do partially overlap. The hydration products of the clinkers produced with partial or total substitution of bauxite (CSAB-Bx/AAS and CSAB-AAS) showed more formation of AFm-type phases. This effect is more pronounced for samples produced

457 using a higher content of AAS. These results are consistent with the XRD data where a
458 reduction in the ettringite content can also be identified after 28 days of curing (Figure
459 4C), as this is partially converted to monosulfate as the reaction progresses. The absence
460 of a defined signal at ~4 ppm suggests the presence of at most a low concentration of
461 AH_3 at 28 days, although this environment might be overlapped by the octahedrally Al
462 coordinated sites of the AFm and AFt phases [82,83]. The aluminium in strätlingite is
463 present in both IV-fold and VI-coordinations, but the presence of alkalis within the
464 structure, mainly for the clinkers produced with AAS, reduces the Al^{IV}/Al^{VI} ratio [84].
465 The signal at 61 ppm for the pastes after 28 days of curing corresponds to the Al^{IV}
466 environment within strätlingite, while its Al^{VI} peak overlaps with those of the other
467 AFm phases present [84]. Therefore, the higher intensity of the peak located at ~10 ppm
468 for the hydrated CSAB-AAS clinkers is attributed to the higher degree of formation of
469 AFm phases including strätlingite, consistent with the diffractograms shown in Figure 4.
470 The presence of residual unreacted ye'elimite even after 28 days of curing is indicated
471 by the lower but non-zero intensity of the main broad peak attributed to Al^{IV} in this
472 phase. Differences in this peak between samples indicate a greater extent of hydration
473 for the CSAB-Bx/AAS and CSAB-AAS clinkers compared to CSAB-Ref.

474 The ^{29}Si MAS NMR spectra for the anhydrous clinkers and their corresponding pastes
475 at 28 days of curing are shown in Figure 7. The spectra for the anhydrous CSAB–Ref
476 and CSAB–Bx/AAS exhibited a narrow resonance at -71 ppm relative to TMS (Q^0 sites)
477 corresponding to the C_2S phase (Figure 7A and B), which is consistent with the XRD
478 results. The CSAB–AAS clinker exhibited a broader peak with a maximum at -71 ppm
479 along with a shoulder located at ~-74 ppm (Figure 7C). These features can be attributed
480 to the tricalcium silicate as identified by XRD in Figure 1. This structure contains nine
481 non-equivalent silicon sites, with overlapping resonances in a spectral range between -

66 and -77 ppm [85], although the presence of paramagnetic ions and different degrees of guest-ion incorporation (such as Mg^{2+}, S^{6+}, Al^{3+}) modify the distribution of silicon-oxygen distances and broaden the ^{29}Si MAS NMR spectra [86]. The peak at -73 ppm in CSAB–Ref (Figure 7A) can be attributed to the presence of ternesite [87].

The ^{29}Si NMR spectra for every paste exhibited residual C_2S from the clinker (resonance at -71 ppm), which is also consistent with the presence of belite in the XRD results. The highest consumption of C_2S is observed for CSAB–Bx/AAS followed by CSAB–AAS. A significant reduction of the characteristic peak attributed to ternesite corroborates its dissolution during hydration. The low content of alite in CSAB–Bx/AAS and CSAB–AAS could lead to the formation of a C-S-H-type phase with short-range order, not identifiable by XRD. The silicate chains in this type of phase show ^{29}Si chemical shifts of -80 to -90 ppm, mainly being present as Q^1, Q^2 and $Q^2(1Al)$ units. Therefore, the weak broad signal around -87 ppm in the samples can be attributed to the presence of both C-S-H and strätlingite [84], and there is a superposition of unresolved signals from these Si environments. The high content of vacancies and/or substitutions in the strätlingite structure tend to decrease the Si connectivity and a more disordered structure can be obtained, which is coherent with the XRD results (Figure 4) showing a broad main strätlingite peak consistent with structural disorder.

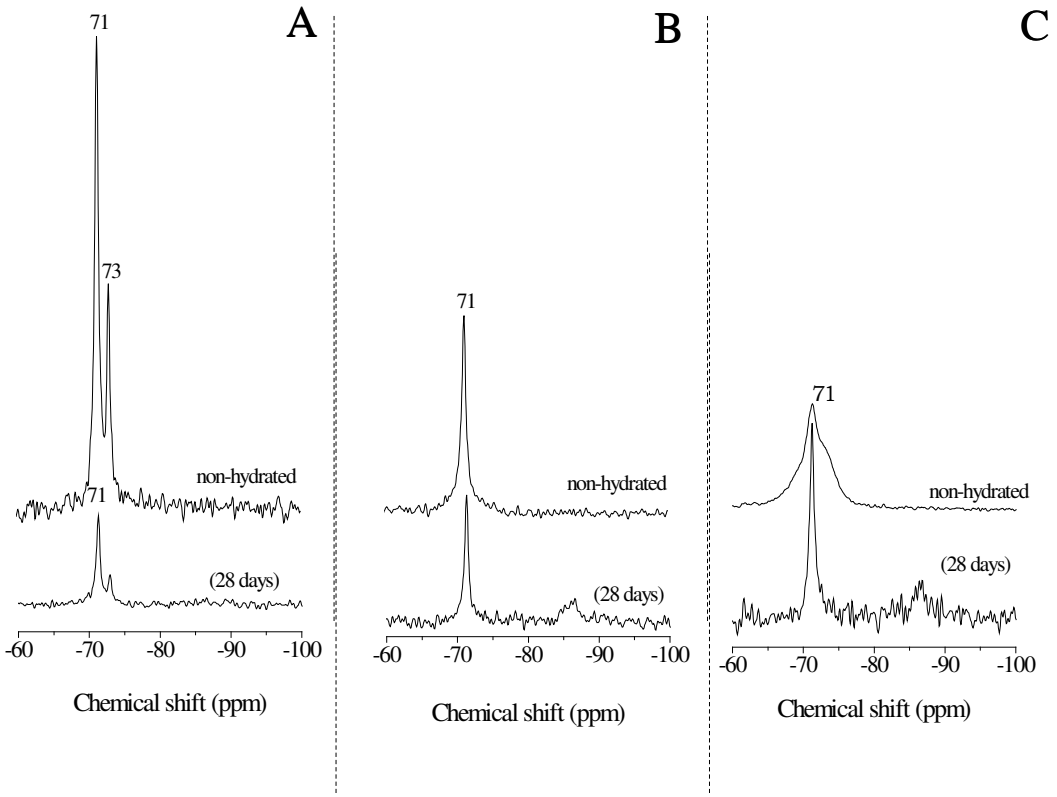

Figure 7. ^{29}Si MAS NMR spectra of anhydrous clinkers and CSAB pastes after 28 days of curing. A. CSAB-Ref; B. CSAB-Bx/AAS and C. CSAB-AAS. Note that the vertical scale for the 28-day cured material in C is exaggerated by a factor of ~2 to emphasise the formation of the new hydrate product peak.

3.2.5. Compressive strength

The results obtained for the mechanical performance of the hydrated pastes of each clinker at different ages of curing are shown in Figure 8. The compressive strengths achieved by the CSAB clinkers produced with the alternative alumina source show a marked difference, despite their similar chemical compositions (Table 3). At early age, CSAB-Bx/AAS shows a compressive strength up to ~32% lower than those of CSAB-AAS and CSAB-Ref. This higher mechanical performance for CSAB-Ref and CSAB-AAS at early age can be attributed to a greater initial extent of hydration, also shown by

514 the higher heat release during the first 24 hours of hydration. The clinkers produced
515 with AAS (CSAB-Bx/AAS and CSAB-AAS) increase their compressive strength by
516 ~70% from 1 day to 7 days of curing, leading to strength performance after 28 days
517 which is considerably higher than that of CSAB-Ref. The growth in compressive
518 strength is also higher with longer-term curing of CSAB-Bx/AAS, which can be
519 attributed to the presence of a higher content of C_2S (see Table 3) contributing to long-
520 term compressive strength development through the formation of strätlinglite [1,16].

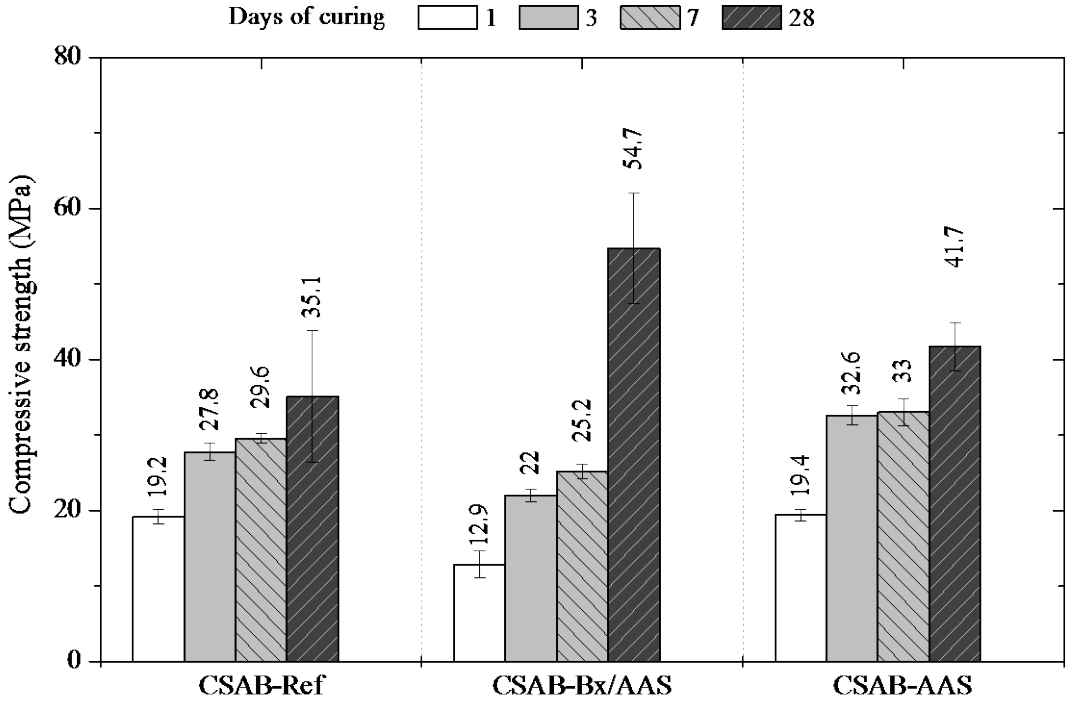

521

522 Figure 8. Compressive strength of C$\bar{S}$AB clinker pastes up to 28 days of curing.

523

524 ## 4. Conclusions

525 This study has demonstrated the potential valorisation of an aluminium anodising
526 sludge – a waste from the aluminium processing industry – as aluminium source in the
527 production of calcium sulfoaluminate-belite (CSAB) clinkers. Ye'elimite and belite

were the main phases formed in clinkerisation, with anhydrite and aluminoferrite-type phases identified as secondary phases. Ternesite was also identified in the reference CSAB clinker produced with mineral reagents, but not when the anodising sludge was used. The use of traditional raw materials (such as bauxite and limestone), as well as an alternative aluminium source has a strong effect on the clinkerisation process as a consequence of the high content of foreign ions, such as Na, K and Mg. As the content of aluminium anodising sludge increases, a higher content of alite is formed. The content of both cubic and orthorhombic ye'elimite is also influenced by the inclusion of aluminium anodising sludge. The ratio between these different polymorphs identified in each of the clinkers synthesised, and the presence of ternesite, appear to play an important role in determining the kinetics of hydration.

Ettringite and calcium monosulfoaluminate hydrate were identified as the main crystalline hydration products in all pastes studied. The presence of belite along with the remaining ye'elimite and/or newly formed amorphous aluminium hydroxide leads to the formation of strätlingite at later ages. These hydrated products, derived from the slightly higher content of belite in the clinkers based on aluminium anodising sludge, contributed to higher compressive strength at 28 days of curing when compared with the reference CSAB clinker.

5. Acknowledgements

This study was sponsored by *Conselho Nacional de Desenvolvimento Científico e Tecnológico* (CNPq) in Brazil and the Universidade Federal Rio Grande do Sul (UFRGS). The authors thank NORIE (*Núcleo Orientado para a Inovação da Edificação*), PANalytical, Escola Politecnica da Universidade de São Paulo (POLI-USP, Brasil), Laboratório da Microestructura e Ecoeficiência

(LME) da Escola Politécnica da USP. The NMR spectra were collected using the EPSRC UK National Solid-state NMR Service at Durham University. The participation of SAB and JLP was funded by a CNPq PVE Fellowship project and by the Royal Academy of Engineering via a Newton Fund grant, and the participation of EDR was funded by a CNPq BJT Fellowship project.

6. References

[1] R. Yang, C.D. Lawrence, J.H. Sharp, Calcium sulfoaluminate cements—low-energy cements, special cements or what?, Adv. Cem. Res. 11 (1999) 3–13. doi:10.1680/adcr.1999.11.1.3.

[2] P.K. Mehta, Investigation on energy-savings cements, World Cem. Technol. 11 (1980) pp 167–177.

[3] M.C.G. Juenger, F. Winnefeld, J.L. Provis, J.H. Ideker, Advances in alternative cementitious binders, Cem. Concr. Res. 41 (2011) 1232–1243. doi:10.1016/j.cemconres.2010.11.012.

[4] F.P. Glasser, L. Zhang, High-performance cement matrices based on calcium sulfoaluminate-belite compositions, Cem. Concr. Res. 31 (2001) 1881–1886. doi:10.1016/S0008-8846(01)00649-4.

[5] Ö. Andaç, F.P. Glasser, Microstructure and microchemistry of calcium sulfoaluminate, Mater. Res. Soc. Symp. Proc. 370 (1995) 135–142.

[6] S. Sahu, J. Majling, Phase compatibility in the system $CaO\text{-}SiO_2\text{-}Al_2O_3\text{-}Fe_2O_3\text{-}SO_3$ referred to sulphoaluminate belite cement clinker, Cem. Concr. Res. 23 (1993) 1331–1339. doi:10.1016/0008-8846(93)90070-P.

[7] G. Álvarez-Pinazo, A. Cuesta, M. García-Maté, I. Santacruz, E.R. Losilla, A.G. De la Torre, et al., Rietveld quantitative phase analysis of ye'elimite-containing cements, Cem. Concr. Res. 42 (2012) 960–971. doi:10.1016/j.cemconres.2012.03.018.

[8] I. Odler, Special Inorganic Cements, First Ed., Taylor and Francis Group, New York,

2000.

[9] Y. Pontikes, G.N. Angelopoulos, Bauxite residue in cement and cementitious applications: Current status and a possible way forward, Resour. Conserv. Recycl. 73 (2013) 53–63. doi:10.1016/j.resconrec.2013.01.005.

[10] E.M. Gartner, L. Guanshu, High belite-containing sulfoaluminous clinker, method for the production and the use thereof for preparing hydraulic binders, US20100132590 A1, 2006.

[11] R.J. Flatt, N. Roussel, C.R. Cheeseman, Concrete: An eco material that needs to be improved, J. Eur. Ceram. Soc. 32 (2012) 2787–2798. doi:10.1016/j.jeurceramsoc.2011.11.012.

[12] G. Álvarez-Pinazo, I. Santacruz, L. León-Reina, M. a G. Aranda, A.G. De La Torre, Hydration reactions and mechanical strength developments of iron-rich sulfobelite eco-cements, Ind. Eng. Chem. Res. 52 (2013) 16606–16614. doi:10.1021/ie402484e.

[13] F. Bullerjahn, D. Schmitt, M. Ben Haha, B. Batog, M. Zajac, Calcium sulfoaluminate cement with ternesite, US20140230697 A1, 2014.

[14] F. Bullerjahn, D. Schmitt, M. Ben Haha, Effect of raw mix design and of clinkering process on the formation and mineralogical composition of (ternesite) belite calcium sulphoaluminate ferrite clinker, Cem. Concr. Res. 59 (2014) 87–95. doi:10.1016/j.cemconres.2014.02.004.

[15] F.P. Glasser, L. Zahng, Calculation of chemical water demand for hydration of calcium sulfoaluminate cement, J. Chinesse Ceram. Soc. 25 (2000) 4340–347.

[16] F.P. Glasser, L. Zhang, High-performance cement matrices based on calcium sulfoaluminate–belite compositions, Cem. Concr. Res. 31 (2001) 1881–1886. doi:10.1016/S0008-8846(01)00649-4.

[17] F. Winnefeld, B. Lothenbach, Hydration of calcium sulfoaluminate cements — Experimental findings and thermodynamic modelling, Cem. Concr. Res. 40 (2010) 1239–1247. doi:10.1016/j.cemconres.2009.08.014.

[18] M. Andac, F.P. Glasser, Pore solution composition of calcium sulfoaluminate cement,

606 Adv. Cem. Res. 11 (1999) 23–26.
607 [19] L. Zhang, F.P. Glasser, Hydration of calcium sulfoaluminate cement at less than 24 h,
608 Adv. Cem. Res. 14 (2002) 141–155.
609 [20] A. Cuesta, G. Álvarez-Pinazo, S.G. Sanfélix, I. Peral, M.A.G. Aranda, A.G. De la Torre,
610 Hydration mechanisms of two polymorphs of synthetic ye'elimite, Cem. Concr. Res. 63
611 (2014) 127–136. doi:10.1016/j.cemconres.2014.05.010.
612 [21] P.-C. Aïtcin, S. Mindess, Binders for Durable and Sustainable Concrete, First Ed.,
613 Taylor & Francis, New Yor, US, 2008.
614 [22] J. Péra, J. Ambroise, New applications of calcium sulfoaluminate cement, Cem. Concr.
615 Res. 34 (2004) 671–676. doi:10.1016/j.cemconres.2003.10.019.
616 [23] S. Peysson, J. Péra, M. Chabannet, Immobilization of heavy metals by calcium
617 sulfoaluminate cement, Cem. Concr. Res. 35 (2005) 2261–2270.
618 doi:10.1016/j.cemconres.2005.03.015.
619 [24] I.A. Chen, M.C.G. Juenger, Incorporation of coal combustion residuals into calcium
620 sulfoaluminate-belite cement clinkers, Cem. Concr. Compos. 34 (2012) 893–902.
621 doi:10.1016/j.cemconcomp.2012.04.006.
622 [25] I. a. Chen, M.C.G. Juenger, Synthesis and hydration of calcium sulfoaluminate-belite
623 cements with varied phase compositions, J. Mater. Sci. 46 (2011) 2568–2577.
624 doi:10.1007/s10853-010-5109-9.
625 [26] I. a. Chen, C.W. Hargis, M.C.G. Juenger, Understanding expansion in calcium
626 sulfoaluminate-belite cements, Cem. Concr. Res. 42 (2012) 51–60.
627 doi:10.1016/j.cemconres.2011.07.010.
628 [27] G. Paul, E. Boccaleri, L. Buzzi, F. Canonico, D. Gastaldi, Cement and concrete research
629 Friedel's salt formation in sulfoaluminate cements: A combined XRD and Al MAS
630 NMR study, Cem. Concr. Res. 67 (2015) 93–102. doi:10.1016/j.cemconres.2014.08.004.
631 [28] G.S. Li, E.M. Gartner, High-belite sulfoaluminate clinker: fabrication process and binder
632 preparation, 04-51586 (publication 2873366), 2006.
633 [29] D. Rockwool, M. Gmbh, C. Ohg, D. Rockwool, Environmental product declaration,

634 ALIPRE-ALICEM. (2012) 1–12.
635 http://www.italcementigroup.com/NR/rdonlyres/F8F160F5-D81B-4722-87BA-
636 1AD23200A1DA/0/EPD_Alipre_042013.pdf (accessed May 10, 2016).
637 [30] Lafarge, Aether ® lower carbon cements, (2015). http://www.aether-cement.eu/
638 (accessed January 1, 2015).
639 [31] W. Dienemann, D. Schmitt, F. Bullerjahn, M. Ben Haha, Belite calciumsulfoaluminate
640 ternesite (BCT): A new low carbon clinker technology, in: 7th Int. VDZ Congr., VDZ
641 Düsseldorf, 2013: pp. 1–19.
642 [32] U.S._Geological_Survey, Mineral commodity summaries: Bauxite and alumina,
643 Washington, D.C., 2015.
644 [33] P. Plunkert, Bauxite and alumina, US Geological Survey Minerals Yearbook (2007) 26-
645 27.
646 [34] J. Beretka, R. Cioffi, M. Marroccoli, G.L. Valenti, Energy-saving cements obtained from
647 chemical gypsum and other industrial wastes, Waste Manag. 16 (1996) 231–235.
648 doi:10.1016/S0956-053X(96)00046-3.
649 [35] R. Cioffi, Environmental and technological effectiveness of a process for the
650 stabilization of a galvanic sludge, J. Hazard. Mater. 89 (2002) 165–175.
651 doi:10.1016/S0304-3894(01)00310-7.
652 [36] S. Sahu, J. Majling, Preparation of sulphoaluminate belite cement from fly ash, Cem.
653 Concr. Res. 24 (1994) 1065–1072. doi:10.1016/0008-8846(94)90030-2.
654 [37] P. Arjunan, M.R. Silsbee, Sulfoaluminate-belite cement from low-calcium fly ash and
655 sulfur-rich and other industrial by-products, Cem. Concr. Res. 29 (1999) 1305–1311.
656 doi:10.1016/S0008-8846(99)00072-1.
657 [38] I. Elkahadiri, A. Diouri, A. Boukhari, F. Puertas, T. Vázquez, Obtaining a
658 sulfoaluminate belite cement by industrial waste, Mater. Constr. 53 (2003) 57–69.
659 [39] Associaçao Brasileira de Normas Técnicas, ABNT NBR10004/2004: Classificção de
660 Resíduos Sólidos (Solid waste - Classification), 2004.
661 [40] M.J. Ribeiro, D.U. Tulyaganov, Recycling of Al-rich industrial sludge in refractory

662 ceramic pressed bodies, Ceram. Int. 28 (2002) 319–326.

663 [41] J.M.F. Ferreira, S.M. Olhero, Al-rich sludge treatments towards recycling, J. Eur.
664 Ceram. Soc. 22 (2002) 2243–2249.

665 [42] A.R. Farinha, R. Mendes, M.T. Vieira, Production of sintered α-alumina by explosive
666 compaction from low temperature calcinated aluminum-rich sludge, Waste and Biomass
667 Valorization. 4 (2013) 627–633. doi:10.1007/s12649-012-9195-6.

668 [43] F. Raupp-Pereira, R.J. Ball, J. Rocha, J.A. Labrincha, G.C. Allen, New waste based
669 clinkers: Belite and lime formulations, Cem. Concr. Res. 38 (2008) 511–521.
670 doi:10.1016/j.cemconres.2007.11.008.

671 [44] F. Raupp-Pereira, D. Hotza, A.M. Segadães, J.A. Labrincha, Ceramic formulations
672 prepared with industrial wastes and natural sub-products, Ceram. Int. 32 (2006) 173–
673 179. doi:10.1016/j.ceramint.2005.01.014.

674 [45] J. Majling, S. Sahu, M. Vlna, D.M. Roy, Relationship between raw mixture and
675 mineralogical composition of sulphoaluminate belite clinkers in the system CaO-SiO_2-
676 Al_2O_3-Fe_2O_3-SO_3, Cem. Concr. Res. 23 (1993) 1351–1356. doi:10.1016/0008-
677 8846(93)90072-H.

678 [46] Y. Nishi, I. Maki, F. Takeuchi, Tricalcium silicate $Ca_3O(SiO_4)$: The monoclinic
679 superstructure, Zeitschrift Fur Krist. (1985) 297–314.

680 [47] K.H. Jost, R. Ziemer, B. Seydel, Redetermination of the Structure of β-dicalcium
681 silicate, Acta Crystallogr. B33 (1977) 1696–1700.

682 [48] G. Redhammer, G. Roth, G. Amthauer, G.J. Tippelt, Srebrodolskite - structural
683 variations in the brownmillerite series $Ca_2(Fe_2\text{-}xAl_x)O_5$, Am. Mineral. 89 (2004) 405–
684 420.

685 [49] W. Saalfeld, H. Depmeier, Yeelimite. Database_code_amcsd 0014178, Krist. Und Tech.
686 7 (1972) 229–233.

687 [50] C.H.L. Calos, A.K. Whittaker, R.L. Davis, N.J. Kennard, Structure of calcium aluminate
688 sulfate Ca4Al6O16S, J. Solid State Chem. 119 (1995) 1–7. doi:10.1016/0022-
689 4596(95)80002-7.

690 [51] E. Iran, G.E. Hentschel, Tillmans, Ternesite, "$Ca_5(SiO_4)_2SO_4$, a new mineral from the
691 Ettringer Bellerberg/Eifel, Germany". ocality: Ettringer Bellerberg volcano, Eifel,
692 Germany. Database_code_amcsd 0014638, Mineral. Petrol. 60 (1997) 121–132.
693 [52] R.B. Hawthorne, F.C. Ferguson, Anhydrous sulphates. Refinement of the crystal
694 structure of anhydrite. Locality: Leopoldshall, East Germany. Database code amcsd
695 0005117, Can. Mineral. 13 (1975) 289–292.
696 [53] R.M. Hazen, Effects of temperature and pressure on the cell dimension and X-ray
697 temperature factors of periclase. Database code_amcsd 0000501, Am. Mineral. 61
698 (1976) 266–271.
699 [54] R.B. Jewell, R.F. Rathbone, T.L. Robl, K.R. Henke, Fabrtication and testing of CSAB
700 cements in mortar and concrete that utilize circulating fluidized bed combustion
701 byproducts, in: World Coal Ash, Lexington, KY, United States, 2009: pp. 1–17.
702 [55] P.K. Mehta, O.E. Gjtcrv, A new test for sulfate resistance of cements, J. Test. Eval. 2
703 (1974) 510–514.
704 [56] J. Majling, D.M. Roy, The potential of fly ash for cement manufacture, Am. Ceram. Soc.
705 Bull. (United States). 72 (1993).
706 [57] X. Liu, Y. Li, N. Zhang, Influence of MgO on the formation of Ca_3SiO_5 and
707 $3CaO.3Al_2O_3.CaSO_4$ minerals in alite – sulphoaluminate cement, Cem. Concr. Res. 32
708 (2002) 1125–1129.
709 [58] Y. Li, X. Liu, S. Li, J. Hu, Influence of P_2O_5 on the formation and hydration properties
710 of C_4A_3S, Mater. Res. Innov. 4 (2001) 241–244. doi:10.1007/PL00010881.
711 [59] K.G. Kolovos, S. Tsivilis, G. Kakali, Study of clinker dopped with P and S compounds,
712 J. Therm. Anal. Calorim. 77 (2004) 759–766.
713 doi:10.1023/B:JTAN.0000041655.82776.09.
714 [60] C.W. Hargis, J. Moon, B. Lothenbach, F. Winnefeld, H.-R. Wenk, P.J.M. Monteiro,
715 Calcium sulfoaluminate sodalite ($Ca_4Al_6O_{12}SO_4$) crystal structure evaluation and bulk
716 modulus determination, J. Am. Ceram. Soc. 97 (2014) 892–898. doi:10.1111/jace.12700.
717 [61] L. Kacimi, M. Cyr, P. Clastres, Synthesis of alpha'L-C_2S cement from fly-ash using the

718 hydrothermal method at low temperature and atmospheric pressure., J. Hazard. Mater.
719 181 (2010) 593–601. doi:10.1016/j.jhazmat.2010.05.054.
720 [62] J. Beretka, B. de Vito, L. Santoro, N. Sherman, G.L. Valenti, Utilisation of industrial
721 wastes and by-products for the synthesis of special cements, Resour. Conserv. Recycl. 9
722 (1993) 179–190. doi:10.1016/0921-3449(93)90002-W.
723 [63] J. Beretka, M. Marroccoli, N. Sherman, G.L. Valenti, The influence of C4A3$ content
724 and ratio on the performance of calcium sulfoaluminate-based cements, Cem. Concr.
725 Res. 26 (1996) 1673–1681. doi:10.1016/S0008-8846(96)00164-0.
726 [64] G. Belz, J. Beretka, M. Marroccoli, L. Santoro, N. Sherman, G.L. Valenti, Use of fly ash,
727 blast furnace slag and chemical gypsum for the synthesis of calcium sulphoaluminate
728 based cements, in: 5th Int. Conf. Fly Ash, Silica Fume, Slag, Nat. Pozzolans Concr.,
729 Milwaukee, WI, 1995: pp. 513–530.
730 [65] V. Makhmudova, M. Iskandarova, Y. Ivanova, G. Chernev, N. Ruziev, Synthesis and
731 properties of sulphoferrite calcium clinkers and low temperature cements on their basis,
732 J. Univ. Chem. Technol. Metall. 46 (2011) 151–154.
733 [66] E. Viggh, N. Menad, B. Björkman, D. Adolfsson, Steelmaking slags as raw material for
734 sulphoaluminate belite cement, Adv. Cem. Res. 19 (2007) 147–156.
735 doi:10.1680/adcr.2007.19.4.147.
736 [67] T.K. Tadzhiev, T.A. Atakuziev, F.K. Tadzhiev, Hardening of anhydrous calcium
737 sulfoaluminate and sulfosilicate, UDC. 691 (1973) 1434–1437.
738 [68] W. Dienemann, F. Bullerjahn, M. Ben Haha, Belite-Calciumsulfoaluminate-ternesite
739 (BTC) - a new low carbon clinker technology, Cem. Int. 11 (2013) 100–109.
740 [69] S. Berger, C.C.D. Coumes, P. Le Bescop, D. Damidot, Influence of a thermal cycle at
741 early age on the hydration of calcium sulphoaluminate cements with variable gypsum
742 contents, Cem. Concr. Res. 41 (2011) 149–160. doi:10.1016/j.cemconres.2010.10.001.
743 [70] I. Jawed, J. Skalny, Alkalies in cement: A review, Cem. Concr. Res. 8 (1978) 37–51.
744 doi:10.1016/0008-8846(78)90056-X.
745 [71] Y. Fu, J.J. Beaudoin, J. Ding, Strätlingite formation in high-alumina cement — zeolite

systems, Adv. Cem. Res. 7 (1995) 171–178. doi:10.1680/adcr.1995.7.28.171.

[72] C.W. Hargis, A. Telesca, P.J.M. Monteiro, Calcium sulfoaluminate (Ye'elimite) hydration in the presence of gypsum, calcite, and vaterite, Cem. Concr. Res. 65 (2014) 15–20. doi:10.1016/j.cemconres.2014.07.004.

[73] L. Pelletier-Chaignat, F. Winnefeld, B. Lothenbach, C.J. Müller, Beneficial use of limestone filler with calcium sulphoaluminate cement, Constr. Build. Mater. 26 (2012) 619–627. doi:10.1016/j.conbuildmat.2011.06.065.

[74] D.G. Evans, R.C.T. Slade, Structural aspects of layered double hydroxides, Struct. Bond. 119 (2006) 1–87. doi:10.1007/430_005.

[75] I. Santacruz, Á.G. De la Torre, G. Álvarez-Pinazo, A. Cabeza, A. Cuesta, J. Sanz, et al., Structure of stratlingite and effect of hydration methodology on microstructure, Adv. Cem. Res. 28 (2016) 13–22.

[76] M. V. Borrachero, J. Payá, M. Bonilla, J. Monzó, The use of thermogravimetric analysis technique for the characterization of construction materials, J. Therm. Anal. Calorim. 91 (2008) 503–509. doi:10.1007/s10973-006-7739-3.

[77] H.J. Kuzel, X-ray investigations of some complex calcium aluminate hydrates and related compounds, in: Tokyo (Ed.), V. Int. Symp. Chem. Cem., 1969: pp. 92–97.

[78] F. Winnefeld, A. Gruskovnjak, R. Figi, B. Lothenbach, U. Mäder, B. Münch, et al., Quantification of hydration phases in supersulfated cements: review and new approaches, Adv. Cem. Res. 23 (2011) 265–275. doi:10.1680/adcr.2011.23.6.265.

[79] J. Skibsted, H.J. Jakobsen, C. Hall, Direct observation of aluminium guest ions in the silicate phases of cement minerals by ^{27}Al MAS NMR spectroscopy, Jorunal Chem. Soc. 90 (1994) 2095–2098.

[80] J. Skibsted, H.J. Jakobsen, C. Hall, Quantitative aspects of ^{27}Al MAS NMR of calcium aluminoferrites, Adv. Cem. Based Mater. 7 (1998) 57–59. doi:10.1016/S1065-7355(97)00017-5.

[81] P. Colombet, A.R. Grimmer, P. Zanni, P. Sozzani, eds., Nuclear Magnetic Resonance Spectroscopy of Cement-Based Materials, Springer Berlin / Heidelberg, Berlin, 1999.

774 [82] G. Le Saout, E. Lécolier, A. Rivereau, H. Zanni, Chemical structure of cement aged at
775 normal and elevated temperatures and pressures, Cem. Concr. Res. 36 (2006) 71–78.
776 doi:10.1016/j.cemconres.2004.09.018.
777 [83] A. Vyalikh, K. Zesewitz, U. Scheler, Hydrogen bonds and local symmetry in the crystal
778 structure of gibbsite., Magn. Reson. Chem. 48 (2010) 877–81. doi:10.1002/mrc.2682.
779 [84] S. Kwan, J. LaRosa, M.W. Grutzeck, ^{29}Si and ^{27}Al MASNMR study of strätlingite, J.
780 Am. Ceram. Soc. 78 (1995) 1921–1926. doi:10.1111/j.1151-2916.1995.tb08910.x.
781 [85] S.L. Poulsen, V. Kocaba, G. Le Saoût, H.J. Jakobsen, K.L. Scrivener, J. Skibsted,
782 Improved quantification of alite and belite in anhydrous Portland cements by ^{29}Si MAS
783 NMR: Effects of paramagnetic ions, Solid State Nucl. Magn. Reson. 36 (2009) 32–44.
784 doi:10.1016/j.ssnmr.2009.05.001.
785 [86] H.F.W. Taylor, Cement Chemistry, Thomas Telford Publishing, London, 1997.
786 [87] L. Bonafous, C. Bessada, D. Massiot, J.P. Coutures, ^{29}Si MAS NMR study of dicalcium
787 silicate: The structural influence of sulfate and alumina stabilizers, J. Am. Ceram. Soc.
788 78 (1995) 2603–2608.
789